Received: 19 July 2022 | Revised: 6 September 2022 | Accepted: 12 September 2022

DOI: 10.1002/jcla.24714

RESEARCH ARTICLE

WILEY

Circular RNA hsa_circ_0018189 drives non-small cell lung cancer growth by sequestering miR-656-3p and enhancing xCT expression

Jianfeng Cai | Yiping Zheng | Lie Dong | Xiangbin Zhang | Yinghui Huang

Department of Respiratory and Critical Care Medicine, Nanping First Hospital Affiliated to Fujian Medical University, Nanping, Fujian, China

Correspondence
Yinghui Huang, Department of Respiratory and Critical Care Medicine, Nanping First Hospital Affiliated to Fujian Medical University, Zhongshan Road 317, Yanping District, Nanping City, Fujian Province, 353006, China.
Email: huangyinghuinpsy@163.com

Abstract

Background: Non-small cell lung cancer (NSCLC) is one of the cancers with a high mortality rate. CircRNAs have emerged as an important regulatory factor in tumorigenesis in recent years. However, the detailed regulatory mechanism of a circular RNA cullin 2 (hsa_circ_0018189; hsa_circ_0018189) is still unclear in NSCLC.

Methods: RNA levels of hsa_circ_0018189, microRNA (miR)-656–3p, and Solute carrier family seven member 11 (SLC7A11, xCT) were analyzed by real-time quantitative reverse transcription-polymerase chain reaction (RT-qPCR), and protein level was assessed by Western blot and immunohistochemical assay. Enzyme-linked immunosorbent assay was conducted to detect cell glutamine metabolism. Effects of hsa_circ_0018189 on cell proliferation, apoptosis, migration, and invasion were analyzed by corresponding assays. Luciferase reporter assay and RNA-immunoprecipitation assay confirmed the target relationship between miR-656-3p and hsa_circ_0018189 or xCT. The in vivo function of hsa_circ_0018189 was verified by xenograft mouse models.

Results: Hsa_circ_0018189 abundance was overexpressed in NSCLC cells and samples. Deficiency of hsa_circ_0018189 lowered NSCLC cell proliferative, migrating, invading, and glutamine metabolism capacities, and hsa_circ_0018189 silencing inhibited the growth of tumors in vivo. Hsa_circ_0018189 could up-regulate xCT by sponging miR-656-3p. And miR-656-3p downregulation or xCT overexpression partly overturned hsa_circ_0018189 knockdown or miR-656-3p mimic-mediated repression of NSCLC cell malignancy.

Conclusion: Hsa_circ_0018189 drove NSCLC growth by interacting with miR-656-3p and upregulating xCT.

KEYWORDS
Hsa_circ_0018189, miR-656-3p, NSCLC, xCT

Jianfeng Cai and Yiping Zheng are contributed equally to this study.

This is an open access article under the terms of the Creative Commons Attribution-NonCommercial-NoDerivs License, which permits use and distribution in any medium, provided the original work is properly cited, the use is non-commercial and no modifications or adaptations are made.
© 2022 The Authors. *Journal of Clinical Laboratory Analysis* published by Wiley Periodicals LLC.

1 | BACKGROUND

Non-small cell lung cancer (NSCLC) is a typical type of lung cancer.[1,2] NSCLC can be further subdivided into adenocarcinoma, squamous cell carcinoma, and large cell carcinoma, depending on the histological differences among the NSCLC subtypes.[3–5] The main risk for NSCLC is smoking.[6] Its poor prognosis and recurrence rate pose great challenges to the treatment of NSCLC.[7,8] Therefore, the research on NSCLC has also become a hot topic today.

Circular RNAs (circRNAs), a class of single-stranded RNA molecules with closed loop structures, have become the focus of RNA and transcriptome research.[9] In fact, circRNAs can be divided into non-coding circRNAs and coding circRNAs.[10,11] Because of their unique structure, they exhibit high stability and resistance to exonucleases.[12] More and more studies on circRNAs in NSCLC have proved the action of circRNAs in the occurrence and development of NSCLC.[13–15] Hsa_circ_0018189 was suggested to exert a significant function in NSCLC,[16] but its specific functional mechanism has not been described.

MiRNA adjusts post-transcriptional gene expression.[17,18] MiRNAs, are key actors in a variety of biological processes, and their disorders have been linked to many diseases, including cancer and autoimmune diseases.[19–21] Dysregulation of miRNAs is common in NSCLC, and miRNAs have been suggested to participate in the regulation of the occurrence, progression, and metastasis of NSCLC by regulating target genes.[22] Therefore, a string of studies has been conducted to explore the functional mechanism of miRNAs in NSCLC, which will also provide the possibility for miRNAs to become a diagnostic and therapeutic tool.[23,24] The functional mechanism of miR-656-3p in NSCLC is not well understood, which makes it of great interest to us.

Solute carrier family seven member 11 (SLC7A11), also named as xCT, is a cystine and glutamate anti-transporter that can transport cystine into cells and export glutamate at the same time.[25,26] It has been reported that elevated xCT expression and glutamate release are commonly detected in cancer cells.[27] xCT has a vital function in the progression of NSCLC, but its specific regulatory mechanism has rarely been reported.

Accordingly, the research was to clarify the changes in hsa_circ_0018189, miR-656-3p, and xCT in NSCLC, and their relationships and functions will be explored. These studies will provide theoretical support for future diagnosis and treatment of NSCLC.

2 | MATERIAL AND METHODS

2.1 | Clinical samples

NSCLC tumor tissues ($N = 90$) and adjacent normal tissues ($N = 90$) were gathered from patients with NSCLC who were diagnosed at Nanping First Hospital Affiliated to Fujian Medical University. The Declaration of Helsinki was referenced in experiments involving human samples. Prior to surgery, the patient was informed and signed informed consent. The experiment was also approved and supported by the Ethics Committee of Nanping First Hospital Affiliated to Fujian Medical University. The tumor tissues were removed and preserved at −80°C.

2.2 | Cell culture and transfection

The BEAS2B cell line (CRL-9609™, ATTC, Manassas, VA) and NSCLC cell lines HCC44 (CBP61182, COBIOER, Nanjing, China) and A549 (CBP60084, COBIOER) were cultured with RPMI-1640 (Sigma-Aldrich, St. Louis, MO) or F12K supplemented with 10% fetal bovine serum (FBS, GIBCO, Carlsbad, CA) in a humidified incubator containing 5% CO_2 at 37°C.

Three small interfering RNAs si-hsa_circ_0018189#1, si-hsa_circ_0018189#2, si-hsa_circ_0018189#3, and negative control (si-NC), miR-656-3p inhibitor and inhibitor NC, miR-656-3p mimic and negative control mimic (mimic NC), pcDNA and pcDNA-xCT, short hairpin RNA targeting hsa_circ_0018189 (sh-hsa_circ_0018189), and negative control (sh-NC) were synthesized and purchased from Sangon Biotech (Shanghai, China). The Lipofectamine 3000 reagent (Invitrogen, Carlsbad, CA) was utilized for transfection according to production instructions.

2.3 | Real-time quantitative reverse transcription-polymerase chain reaction and validation of circular characteristics

The TRIzol® Reagent (Invitrogen) was utilized for isolation of total RNA. Complementary DNA (cDNA) was synthesized using First-Strand cDNA Synthesis Kit (Takara, Dalian, China). SYBR® Premix DimerEraser Kit (Takara, Dalian, China) was utilized to detect relative expression. The $2^{-\Delta\Delta Ct}$ method[28] was applied to process relative expression and β-actin or U6 was applied for standardization.[29,30] The primers are shown in Table 1.

The extracted total RNA was digested by adding 10 μl RNase R for subsequent analysis. Meanwhile, cells were treated with

TABLE 1 Primers sequences used for PCR

Name	Primers for PCR (5'-3')	
hsa_circ_0018189 (circCUL2)	Forward	TTGCAAAGCACCTGAACTGC
	Reverse	CTCGGAGCAGCATTCGGATA
SLC7A11	Forward	AAGGTGCCACTGTTCATCCC
	Reverse	TGTTCTGGTTATTTTCTCCGACA
miR-656-3p	Forward	GCCGAGAATATTATACAGTCA
	Reverse	CTCAACTGGTGTCGTGGAG
miR-888-5p	Forward	GCCGAGTACTCAAAAAGCTGT
	Reverse	CTCAACTGGTGTCGTGGAG
β-actin	Forward	CTTCGCGGGCGACGAT
	Reverse	CCACATAGGAATCCTTCTGACC
U6	Forward	CTCGCTTCGGCAGCACA
	Reverse	AACGCTTCACGAATTTGCGT
CUL2	Forward	TGGTGCCTGGCAAGGAATTT
	Reverse	ATTCCAACATGACCACGGCT

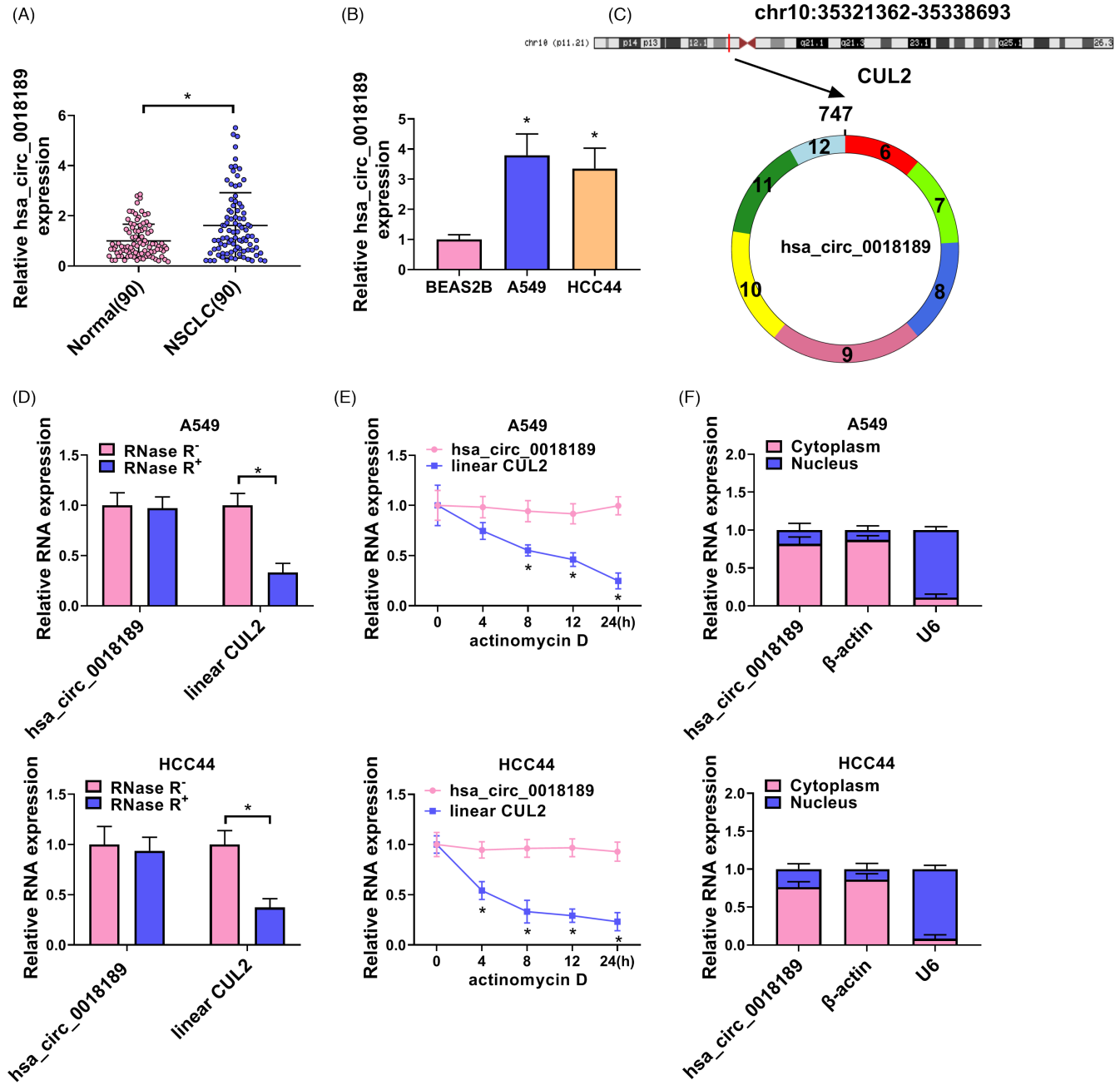

FIGURE 1 Upregulation of hsa_circ_0018189 expression was acquired in NSCLC. (A) RT-qPCR analyzed hsa_circ_0018189 abundance in NSCLC tissues and normal tissues; (B) Hsa_circ_0018189 abundance in BEAS2B, A549, and HCC44 cells; (C) The location and structure of hsa_circ_0018189 were shown; (D) After RNase R digestion, RT-qPCR was conducted to analyze hsa_circ_0018189 and linear CUL2 expression; (E) After the cells were treated with actinomycin D for 0, 4, 8, 12, and 24 h, RT-qPCR was conducted to detect hsa_circ_0018189 and linear CUL2 expression; (F) The localization of circCUL2 in NSCLC cells was analyzed by subcellular fractionation with RT-qPCR analysis. *$p < .05$

actinomycin D for 0, 4, 8, 12, and 24 h, respectively, and RNA was extracted for subsequent analysis.

2.4 | Glutamine metabolism analysis

Glutamine metabolism was assessed by intracellular levels of glutamine, glutamate, and α-KG. In 6-well plates, the transfected cells were fed. After 24 h, the intracellular correlation levels were determined and analyzed using ELISA kits (Beyotime, Shanghai, China) including glutamine, glutamate, and α-KG according to the instructions.

2.5 | Cell Counting Kit-8 assay

In 96-well plates, the transfection of cells was cultured for 24 h, and 10 μl Cell Counting Kit-8 (CCK8, Beyotime, Shanghai, China) reagent

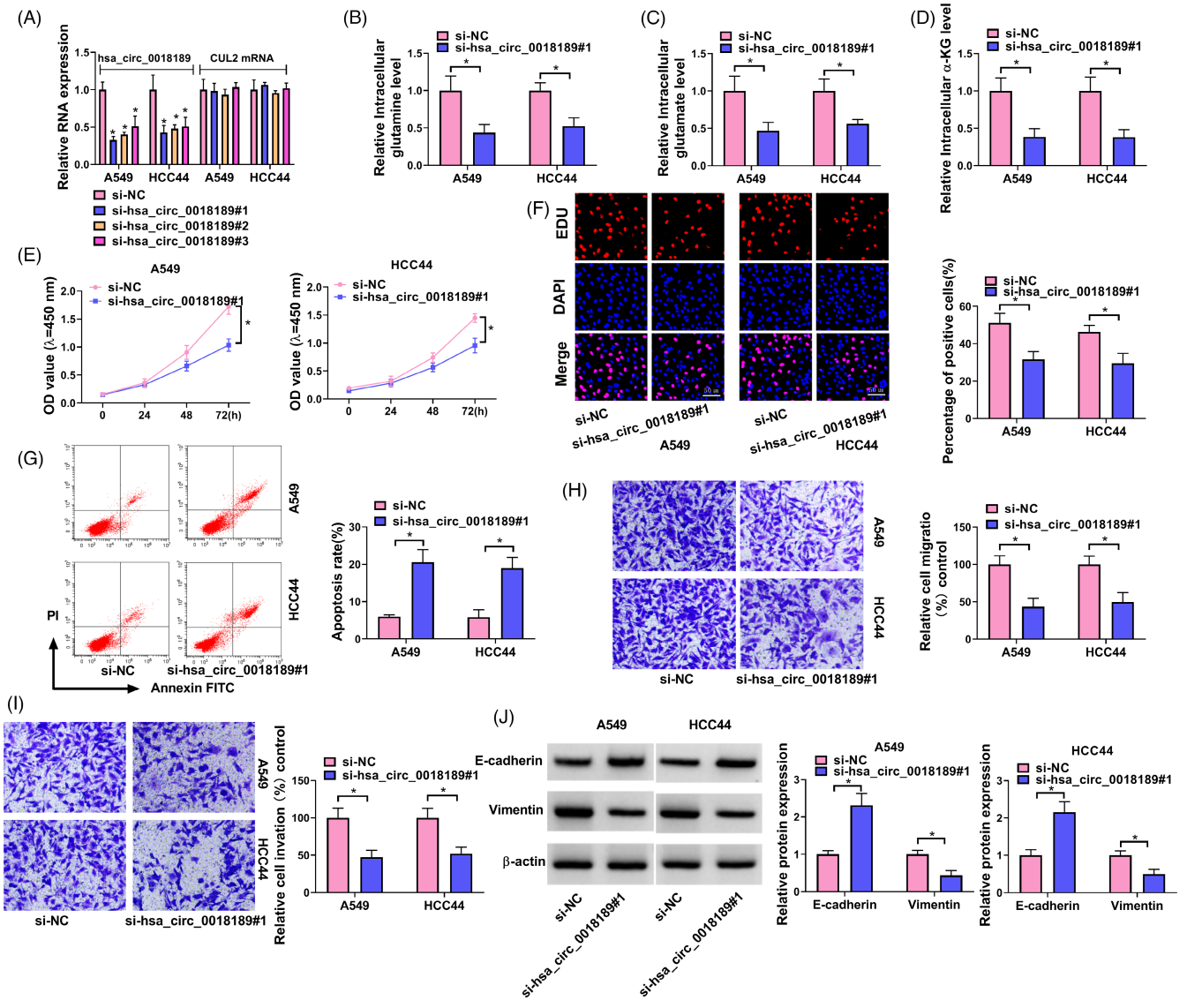

FIGURE 2 Silencing of hsa_circ_0018189 could inhibit glutamine metabolism, proliferation, migration, and invasion, while promote cell apoptosis in NSCLC cells. (A) The transfection efficiency of si-hsa_circ_0018189#1, si-hsa_circ_0018189#2, and si-hsa_circ_0018189#3 were analyzed by RT-qPCR in A549, and HCC44 cells; (B-D) ELISA assay analyzed glutamine metabolism after transfection of si-NC or si-hsa_circ_0018189#1; (E) Cell viability in the above cells was analyzed by CCK8 assay; (F) Cell proliferation was analyzed by EdU assay; (G) Cell apoptosis was analyzed by flow cytometry assay; (H and I) Cell migration and invasion were analyzed by Transwell assay; (J) Proteins of E-cadherin and Vimentin were measured. $^{*}p < .05$

was added to each well to hatch for 24, 48, and 72 h. Then, optical density (OD) was recorded at 450 nm by a microplate reader.

2.6 | 5-ethynyl-2′-deoxyuridine assay

Cell proliferative capacity was estimated with the EdU Staining Proliferation Kit (Abcam, Cambridge, UK). After transfection, the cells were continued to be cultured in 6-well plates, and 10 μl EdU (5-ethynyl-2′-deoxyuridine) reagent was added into the cells for further incubation for 2 h. Then, the medium was discarded. The cells were stained with the stain for 30 min. Then DAPI was applied for staining for 20 min. Finally, the cells were cleaned and observed and analyzed under a microscope.

2.7 | Cell apoptosis analysis

Cell apoptotic rate was estimated with an Annexin V-FITC/PI Staining Kit (Roche, Switzerland) on a flow cytometry (Beckman Coulter; Kraemer Boulevard, CA) following the processes offered by the manufacturer.

2.8 | Cell migration and invasion analysis

The cells were prepared into cell suspension. For the migration experiment, transfected cells resuspended in 200 μl of serum-free medium were complemented in the upper chamber. For the invasion experiment, transfected cells were complemented in the upper chamber

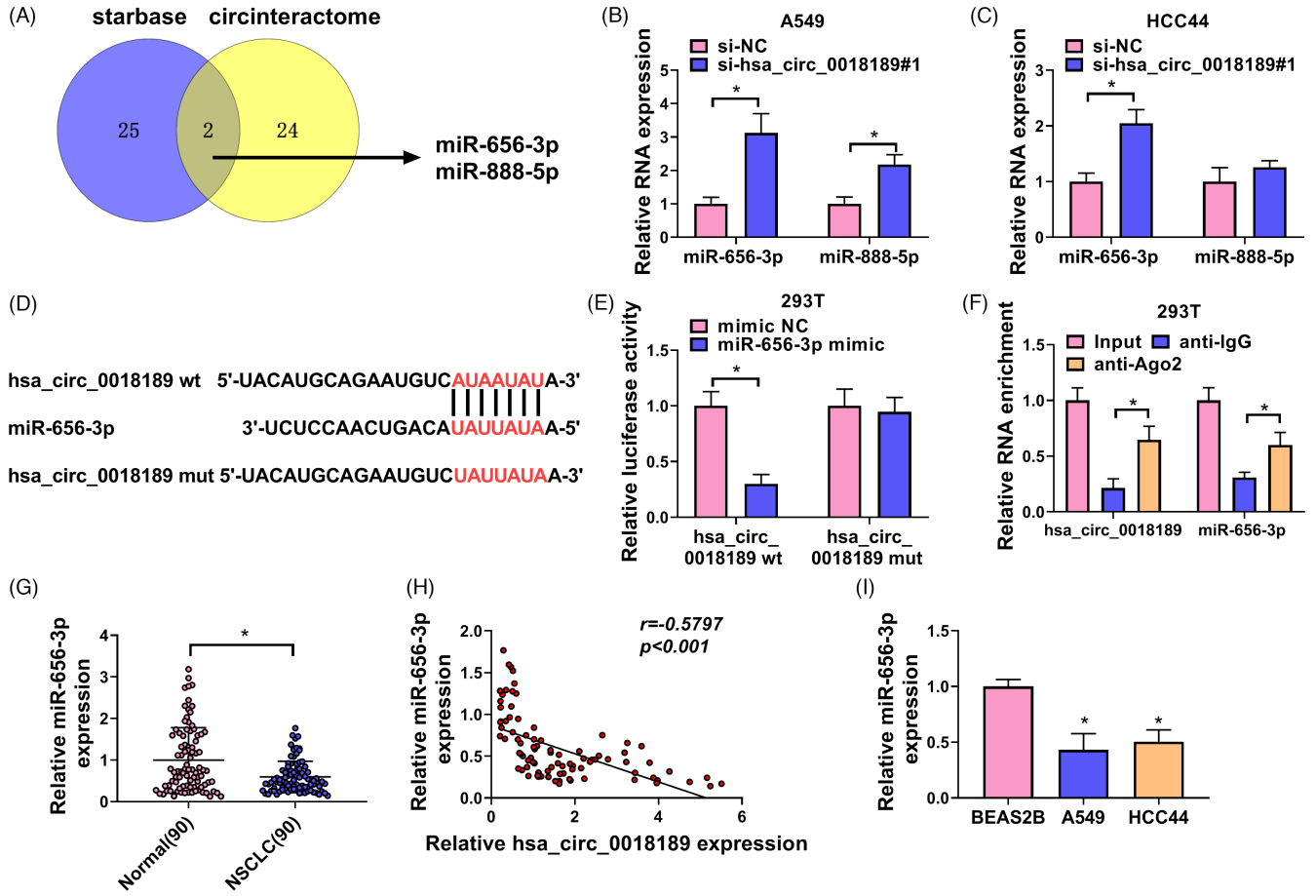

FIGURE 3 Hsa_circ_0018189 acted as a miR-656-3 sponge. (A) Starbase and circinteractome showed the predicted target miRNAs for hsa_circ_0018189; (B and C) RNA levels of miR-656-3p and miR-888-5p were determined after transfection of si-NC or si-hsa_circ_0018189#1; (D) The binding sites of hsa_circ_0018189 and miR-656-3p; (E and F) Luciferase reporter assay and RIP assay were utilized to analyze the interaction of hsa_circ_0018189 and miR-656-3p in 293T cells; (G) RT-qPCR was used to analyze miR-656-3p level in NSCLC tissues and normal tissues; (H) Pearson correlation coefficient was used to analyze the correlation of miR-656-3p and hsa_circ_0018189; (I) RT-qPCR was used to analyze miR-656-3p expression in BEAS2B, A549 and HCC44 cells. *$p < .05$

pre-coated with matrigel (Corning, New York, Madison). 500 μl of medium containing 10% FBS was complemented in the lower chamber. Twenty-four hours later, cells that migrated or invaded were fixed with 4% paraformaldehyde and then stained with crystal violet for 30 min. Cells were counted using an inverted microscope.

2.9 | Western blot

RIPA lysis buffer (Beyotime, Shanghai, China) supplemented with protease inhibitors (Roche, Switzerland) was used to isolate total protein from NSCLC tissues and cells. After treatment, proteins were separated by sodium dodecyl sulfate-polyacrylamide gel electrophoresis. The isolated protein was then transferred onto PVDF (Millipore, Billerica, MA) membrane, and then, the protein-carrying membranes were probed with a primary antibody against E-cadherin (ab1416 at a dilution of 1:50, Abcam), Vimentin (ab8069, 1 μg/ml, Abcam), β-actin (ab8226, 1 μg/ml, Abcam), or xCT (ab175186 at a dilution of 1:1000, Abcam) for 2 h at room temperature, followed by incubation with a secondary antibody. Finally, the ECL Kit (Beyotime, Shanghai, China) was used for band observation and analysis.

2.10 | Luciferase reporter assay and RNA-immunoprecipitation assay

The sequences of hsa_circ_0018189 and 3'untranslated region of xCT (xCT 3'UTR) containing the wild-type (wt) miR-656-3p binding site were cloned into pmirGLO Expression vectors (Promega, Madison, WI), and the mutant type (mut) miR-656-3p binding site was performed based on the hsa_circ_0018189 wt and xCT 3'UTR wt vectors via QuikChange II Site-Directed Mutagenesis Kit (Stratagene, Santa Clara, CA). Co-transfection of wt/mut reporter vector and miR-656-3p mimic or mimic NC was performed. The transfected cells were collected and fully lysed, followed by low-temperature and high-speed centrifugation to collect the supernatant, which was then plated into the 96-well plate in triplicate for the

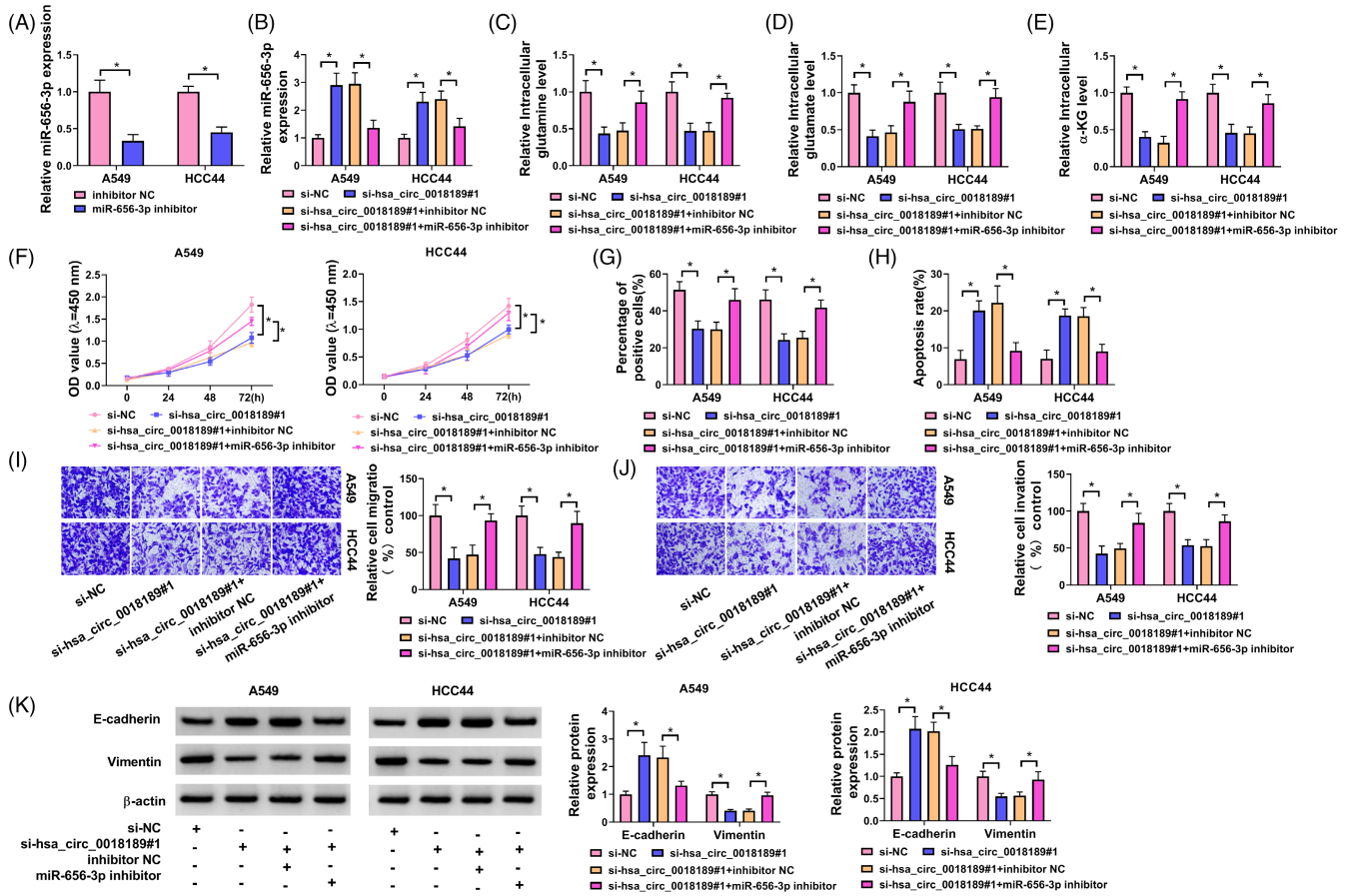

FIGURE 4 MiR-656-3p could restore the effect of hsa_circ_0018189 knockdown on NSCLC progression. (A) MiR-656-3p abundance was detected after transfection of inhibitor NC and miR-656-3p inhibitor; (B-K) Cells were transfected with si-NC, si-hsa_circ_0018189#1, si-hsa_circ_0018189#1 + inhibitor NC, or si-hsa_circ_0018189#1 + miR-656-3p inhibitor. (B) MiR-656-3p expression was estimated after transfection; (C-E) ELISA assay analyzed glutamine metabolism after transfection; (F and G) Cell proliferation was determined; (H) Cell apoptosis was assessed after transfection; (I and J) Cell migrating and invading abilities were analyzed; (K) E-cadherin and Vimentin protein levels were determined. $^{*}p < .05$

measurement of the luciferase activity using the luciferase reporter system (Promega).

RIP-Assay Kit (Millipore) was used to perform RIP assay as per the manufacturer's instructions. After the beads were cleaned with cleaning buffer, pre-diluted anti-IgG (Abcam) or anti-Ago2 (Abcam) solution was added to them and incubated at low temperature for 2 h. Cells were fully lysed after 48 h of transfection. The supernatant was incubated with the beads conjugated with antibodies at 4°C overnight. Then, the beads were collected by centrifugation at low temperatures and low speeds. RNA samples cleared from the beads were used for subsequent analysis of hsa_circ_0018189 and miR-656-3p.

2.11 | Xenograft mice model

All procedures and animal experiments were approved by the Animal Ethics Committee of Nanping First Hospital Affiliated to Fujian Medical University. A549 cells stable expressing sh-hsa_circ_0018189 or sh-NC were subcutaneously injected into four-week-old BALB/c nude mice (Vital River Laboratory Animal Technology [Beijing, China]). Tumor volumes ($0.5 \times (\text{width})^2 \times \text{length}$) were measured every week for four weeks, and tumor weights were analyzed after the mice were euthanized.

2.12 | Immunohistochemistry assay

Freshly removed tissues were paraffin sectioned, dewaxed, and repaired, followed by incubation with 0.3% hydrogen peroxide. After incubation with a primary antibody (ki-67 or xCT) and a secondary horseradish peroxidase antibody, color was developed using DAB solution. Each sample selected five fields for observation.

2.13 | Statistical analysis

All data were statistically examined by GraphPad 7.0. All the data were presented as mean ± standard deviation (SD). $p < .05$ was considered statistically significant. We used a two-tailed Student's *t* test (two groups) and one-way or two-way analysis of variance with

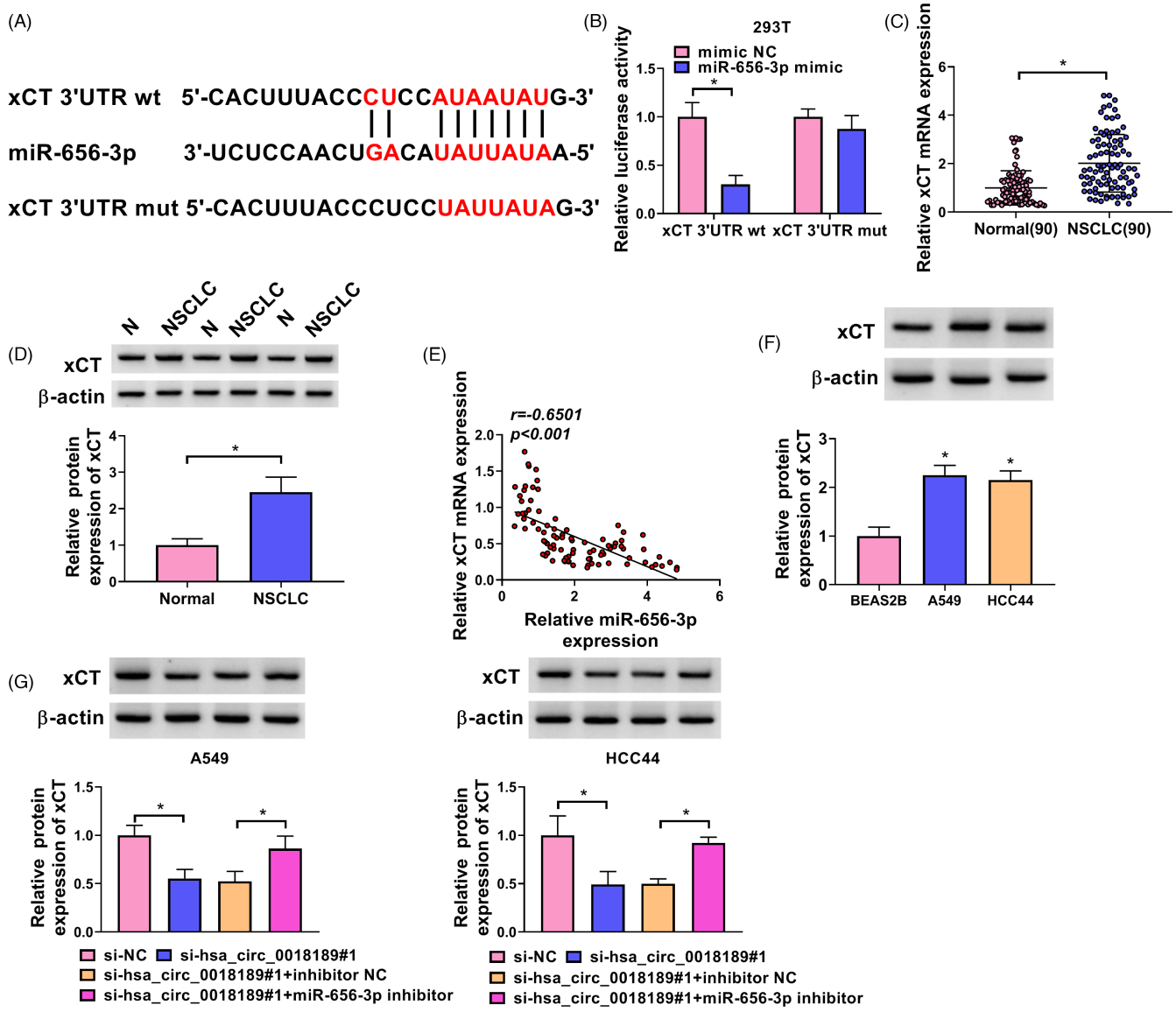

FIGURE 5 There was a target relationship between miR-656-3p and xCT. (A) The binding sites of miR-656-3p and xCT; (B) Luciferase reporter assay tested the luciferase activities of xCT 3'UTR wt and xCT 3'UTR mut in 293T cells after transfection of mimic NC or miR-656-3p mimic; (C) RNA levels of xCT in NSCLC samples; (D) Protein levels of xCT in NSCLC samples; (E) The correlation of miR-656-3p and xCT mRNA expression levels in NSCLC samples; (F) Protein levels of xCT in BEAS2B, A549, and HCC44 cells; (G) Protein levels of xCT were estimated after transfection of si-NC, si-hsa_circ_0018189#1, si-hsa_circ_0018189#1 + inhibitor NC, or si-hsa_circ_0018189#1 + miR-656-3p inhibitor. *$p < .05$

Tukey's post hoc test (more than two groups) to compare significant differences.

3 | RESULTS

3.1 | Upregulation of hsa_circ_0018189 expression was detected in NSCLC

Firstly, we analyzed the expression of hsa_circ_0018189 in NSCLC samples. Hsa_circ_0018189 was observed to be boosted in NSCLC samples (Figure 1A). Meanwhile, compared with BEAS2B, circLUC2 abundance was boosted in A549 and HCC44 cells (Figure 1B). Subsequently, we found that hsa_circ_0018189 was located at chr10 chromosome and was derived from the exons 6–12 of CUL2 mRNA (Figure 1C). We then verified the circular structure of hsa_circ_0018189. Also, hsa_circ_0018189 abundance was not significantly changed but linear CUL2 was reduced in A549 and NCC44 cells with RNase R treatment (Figure 1D). Additionally, hsa_circ_0018189 abundance had no difference after actinomycin D treatment (Figure 1E). Subcellular fractionation with RT-qPCR analysis showed that hsa_circ_0018189 was mainly distributed in the cytoplasm of NSCLC cells (Figure 1F). In short, hsa_circ_0018189 was significantly upregulated in NSCLC.

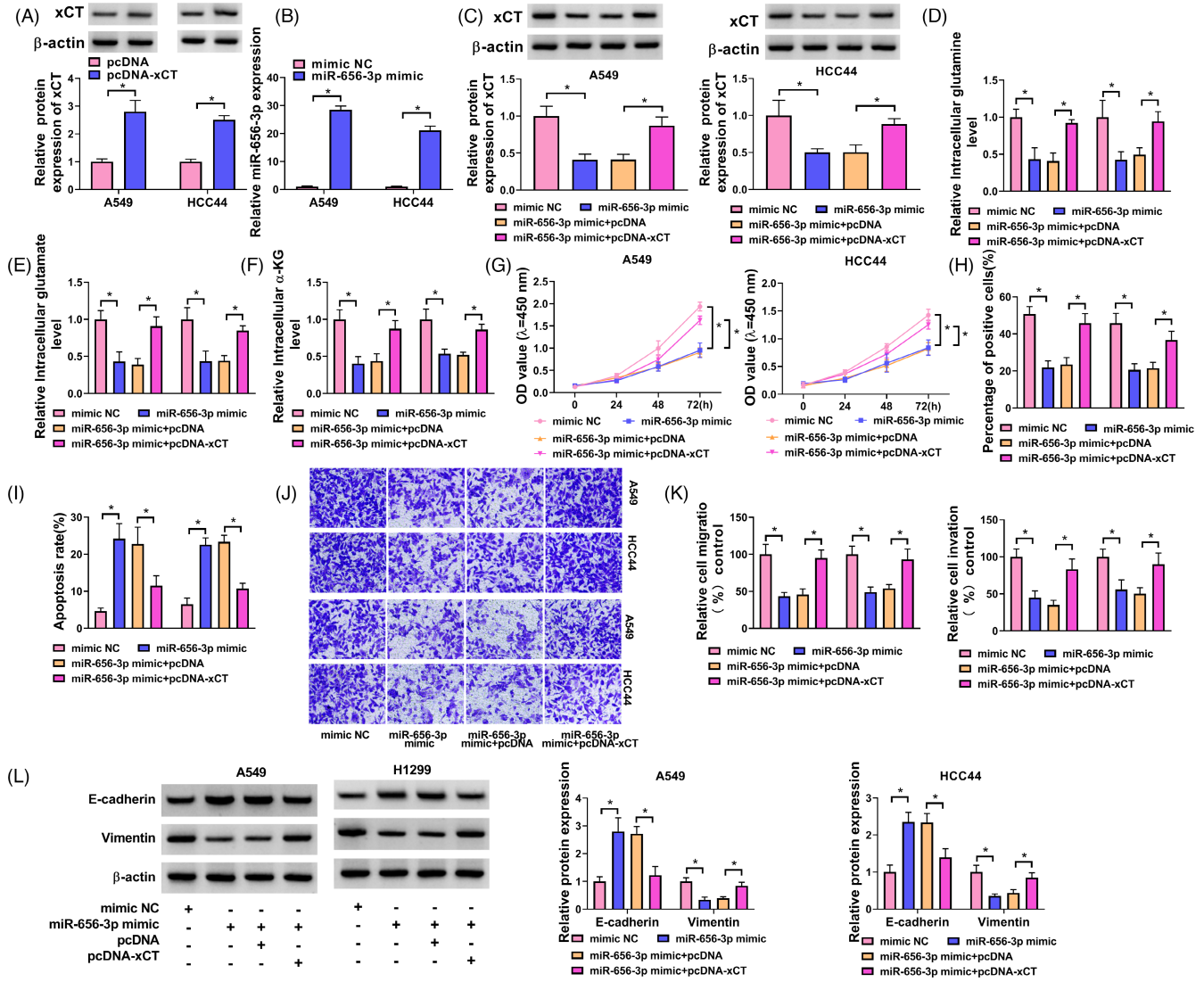

FIGURE 6 Overexpression of xCT could recover miR-656-3p-urged impacts on NSCLC progression. (A) Protein levels of xCT protein were tested after transfection of pcDNA and pcDNA-xCT; (B) MiR-656-3p abundance was determined after transfection of miR-656-3p mimic and mimic NC; (C) Protein levels of xCT were detected after transfection mimic NC, miR-656-3p mimic, miR-656-3p mimic+pcDNA, or miR-656-3p mimic+pcDNA-xCT; (D-F) Glutamine metabolism in the above cells was analyzed; (G and H) Cell proliferation in the above cells was estimated; (I) Cell apoptosis in the above cells was detected; (J and K) Cell migration and invasion in the above cells were determined; (L) E-cadherin and Vimentin protein levels in the above cells were measured. $^{*}p < .05$

3.2 | Hsa_circ_0018189 knockdown suppressed glutamine metabolism, cell proliferation, migration, and invasion, while enhanced cell apoptosis in NSCLC cells

At first, we verified the action of hsa_circ_0018189 knockdown, and the results suggested that si-hsa_circ_0018189#1 caused the greatest silencing efficiency of hsa_circ_0018189 in both cells (Figure 2A). Hence, we used si-hsa_circ_0018189#1 to exhibit the next experiments. We found that knockdown of hsa_circ_0018189 could inhibit glutamine metabolism (Figure 2B, C, and D). CCK8 assay and EdU assay confirmed that lowered hsa_circ_0018189 expression restrained cell proliferation of A549 and HCC44 cells (Figure 2E, F). In addition, cell apoptosis was increased after hsa_circ_0018189 knockdown (Figure 2G). Transwell assay results proved that si-CUL2#1 could suppress cell migration and invasion of A549 and HCC44 cells (Figure 2H, I). E-cadherin and Vimentin are mesenchymal markers commonly used in scientific research for epithelial–mesenchymal transformation (EMT). Knockdown of hsa_circ_0018189 promoted E-cadherin level and retrained protein level of Vimentin in A549 and HCC44 cells (Figure 2J). We also constructed the hsa_circ_0018189 overexpression plasmid, as shown in Figure SS1. In contrast, hsa_circ_0018189 overexpression elevated glutamine metabolism, facilitated cell proliferation, migration, invasion, and lowered cell apoptosis

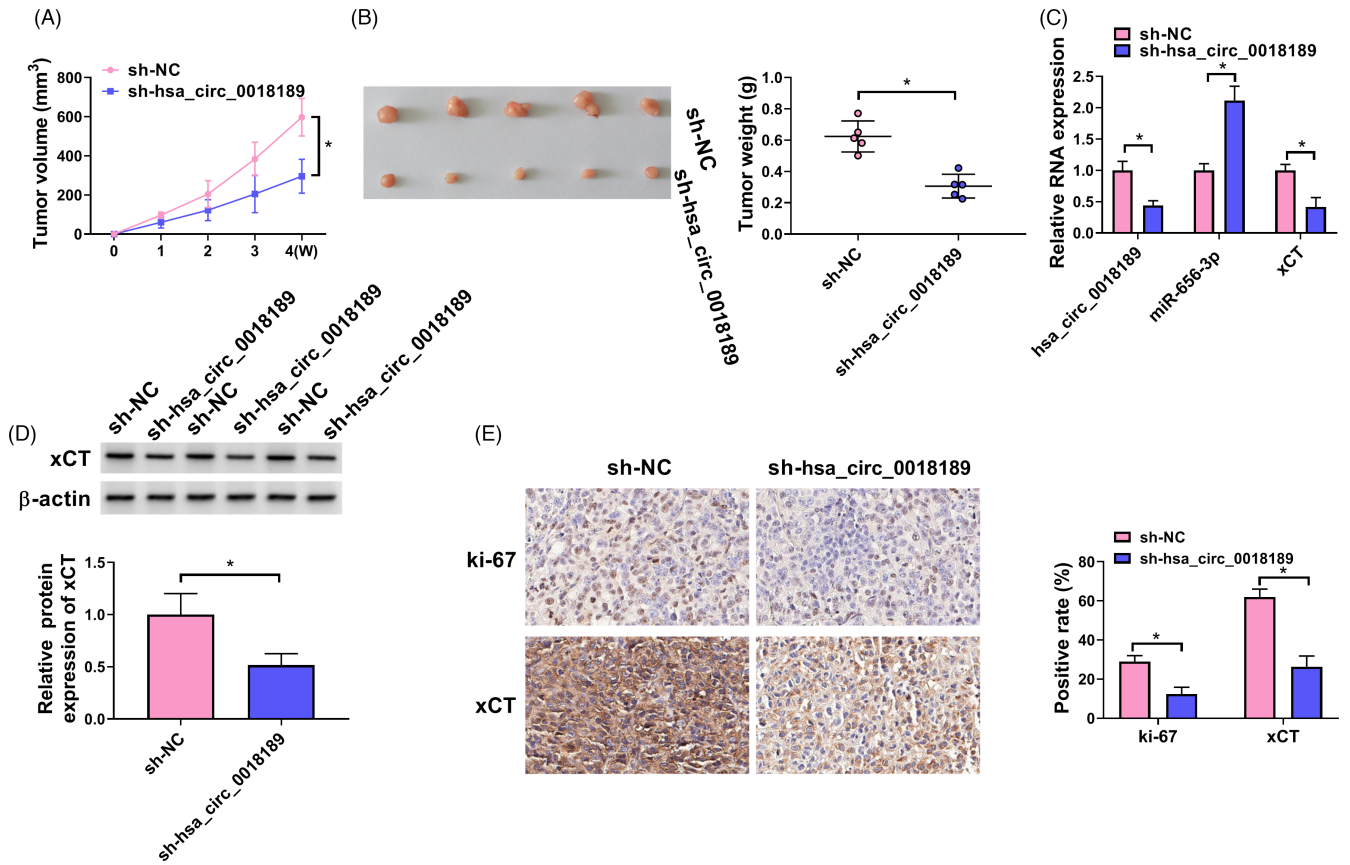

FIGURE 7 Knockdown hsa_circ_0018189 could inhibit the growth of tumors in vivo. (A) The tumor volumes were measured at 1, 2, 3, and 4 weeks; (B) Tumor weights were tested; (C) RNA levels of hsa_circ_0018189, miR-656-3p, and xCT in xenograft tumor tissues were analyzed; (D) Protein levels of xCT in xenograft tumor tissues were determined; (E) IHC analysis of ki-67 and xCT protein levels in xenograft tumor tissues. $^{*}p < .05$

in NSCLC cells (Figure SS1B-I). Consistently, hsa_circ_0018189 overexpression elevated Vimentin protein levels and lessened E-cadherin protein levels (Figure SS1J and K). All in all, these data implied that hsa_circ_0018189 promoted the progression of NSCLC.

3.3 | Hsa_circ_0018189 was identified as a miR-656-3p molecular sponge

Starbase and circinteractome analysis found that miR-656-3p and miR-888-5p were the most promising targets for hsa_circ_0018189 (Figure 3A). Hsa_circ_0018189 silencing resulted in an elevation in miR-656-3p expression level (Figure 3B, C), which was chosen for subsequent research. By using the Starbase database, we predicted the existence of targeted binding sites between hsa_circ_0018189 and miR-656-3p (Figure 3D). Luciferase reporter assay and RIP assay demonstrated the interaction between hsa_circ_0018189 and miR-656-3p in 293T cells (Figure 3E, F). MiR-656-3p expression was lower in NSCLC tissues (Figure 3G). Pearson correlation analysis showed that hsa_circ_0018189 and miR-656-3p were negatively correlated with each other in NSCLC tumors (Figure 3H). MiR-656-3p abundance was lower in A549 and HCC44 cells (Figure 3I). All findings testified that hsa_circ_0018189 could target miR-656-3p.

3.4 | Hsa_circ_0018189 sponged miR-656-3p to promote cell glutamine metabolism and malignancy in NSCLC cells

The silencing effect of miR-656-3p was significant by miR-656-3p inhibitor (Figure 4A). Knockdown of hsa_circ_0018189-mediated elevation of miR-656-3p could be restored after miR-656-3p silencing (Figure 4B). Deficiency of miR-656-3p could relieve the function of si-hsa_circ_0018189#1 on glutamine metabolism (Figure 4C–E). The results of CCK8 assay and EdU assay also expounded that miR-656-3p silencing recover si-hsa_circ_0018189#1-caused repression of A549 and HCC44 cell proliferation (Figure 4F, G). Moreover, transfection of miR-656-3p inhibitor attenuated the role of si-hsa_circ_0018189#1 on cell apoptosis, migration, and invasion (Figure 4H, I, and J). E-cadherin and Vimentin proteins expression were influenced by si-hsa_circ_0018189#1, while miR-656-3p could abolish the influence (Figure 4K). Taken together, the evidence

implied that hsa_circ_0018189 could interact with miR-656-3p to reinforce NSCLC cell glutamine metabolism and malignancy.

3.5 | MiR-656-3p directly interacted with xCT

Using the TargetScan, we revealed that xCT 3'UTR harbored putative target sequences for miR-656-3p (Figure 5A). Luciferase reporter experiment suggested that in 293T cells, miR-656-3p could reduce the luciferase activity of wild-type xCT 3'UTR group, while there was no significant difference in mutant xCT 3'UTR (Figure 5B), confirming the targeting relationship between miR-656-3p and xCT. The mRNA and protein levels of xCT were predominantly raised in NSCLC rather than in normal tissues (Figure 5C, D). xCT mRNA expression in NSCLC samples was negatively correlated with miR-656-3p (Figure 5E). Besides, xCT protein levels were upregulated in A549 and HCC44 cells (Figure 5F). Additionally, xCT expression was decreased after knockdown of hsa_circ_0018189, while miR-656-3p downregulation could restore the function of si-hsa_circ_0018189#1 on xCT expression in A549 and HCC44 cells (Figure 5G). In summary, our findings elucidated that miR-656-3p could target xCT, and hsa_circ_0018189 could regulate the expression of xCT by acting as a sponge of miR-656-3p in NSCLC.

3.6 | MiR-656-3p could inhibit cell glutamine metabolism and malignancy by reducing xCT expression in NSCLC

Introduction of xCT upregulated xCT protein levels in A549 and HCC44 cells (Figure 6A). MiR-656-3p abundance was increased after transfection of miR-656-3p mimic (Figure 6B). The lowered xCT protein levels urged by miR-656-3p overexpression were recovered after xCT introduction (Figure 6C). Besides, xCT upregulation impaired the role of miR-656-3p mimic on factors associated with glutamine metabolism (Figure 6D, E and F). Beyond that, CCK8 assay and EdU assay analysis manifested that introduction of pcDNA-xCT weakened the action of miR-656-3p on A549 and HCC44 cell proliferation and apoptosis (Figure 6G, H, and I). The lowered migrating and invading capacities driven by miR-656-3p were lessened after xCT overexpression (Figure 6J, K). Moreover, miR-656-3p-mediated changes in E-cadherin and Vimentin protein levels were recovered by co-transfection of xCT and miR-656-3p (Figure 6L). In a word, the effect of miR-656-3p could be impaired by xCT in regulating the processes of NSCLC cells.

3.7 | Hsa_circ_0018189 could regulate tumor growth in mouse models

The A549 cells stable expressing sh-hsa_circ_0018189 were subcutaneously injected into the nude mice. Tumor volume expression in mice was measured. Hsa_circ_0018189 knockdown inhibited tumor volume (Figure 7A). The results showed that knocking down hsa_circ_0018189 reduced tumor volume (Figure 7B). RNA levels of hsa_circ_0018189 and xCT were downregulated in xenograft tumor tissues from the sh-hsa_circ_0018189 group, but miR-656-3p expression was increased (Figure 7C). Western blot analysis suggested that xCT protein was decreased in xenograft tumor tissues with hsa_circ_0018189 silence (Figure 7D). IHC analysis revealed that ki-67 and xCT levels were reduced in xenograft tumor tissues with hsa_circ_0018189 silence (Figure 7E). All data exposed that knockdown of hsa_circ_0018189 could inhibit the growth of tumors in vivo.

4 | DISCUSSION

NSCLC is one of the cancers with high mortality in the world.[31] The treatment of NSCLC has made great progress in the continuous development of science and technology condition.[32] However, poor prognosis is still a difficult problem in the treatment of lung cancer today. The functional mechanism of circRNAs in many cancers has been confirmed.[33] The high level of hsa_circ_0018189 in tissues and cells of NSCLC aroused our interest in the detailed functional mechanism of hsa_circ_0018189 in NSCLC. In the present research, we confirmed that hsa_circ_0018189 was highly expressed in NSCLC tissues and cells, which led us to speculate that the upregulation of hsa_circ_0018189 might be a key factor leading to tumorigenesis. Further investigation found that cell proliferation, migration, invasion, and glutamine metabolism were inhibited under hsa_circ_0018189 knockdown condition, but cell apoptosis was significantly induced. In mouse xenograft experiments, hsa_circ_0018189 knockdown lessened NSCLC cell growth in vivo. These results preliminarily confirmed that hsa_circ_0018189 could promote the development of NSCLC.

The regulatory role of hsa_circ_0018189 in NSCLC has been confirmed, but its specific mechanism has not been reported,[16] so we did further exploratory experiments. Starbase prediction revealed that miR-656-3p might interact with hsa_circ_0018189. Further experiments confirmed that hsa_circ_0018189 functioned as a miR-656-3p sponge molecular. Low level of miR-656-3p has been reported in various tumors, such as hepatocellular carcinoma, nasopharyngeal cancer, and colorectal cancer.[34–36] A previous study exhibited that miR-656-3p was downregulated in NSCLC samples and cell lines, and miR-656-3p overexpression lessened cell malignancy.[37] In this research, we also verified the downregulation of miR-656-3p in NSCLC samples and cell lines, and the reduced miR-656-3p expression was able to restore the effects of si-hsa_circ_0018189#1 on NSCLC progression. These results confirmed that hsa_circ_0018189 could promote the development of NSCLC cells by targeting miR-656-3p.

The role of xCT as an intermediate glutamate transporter in NSCLC had also been well reported.[38] In our experiment, xCT abundance was significantly upregulated in NSCLC cells and samples, and miR-656-3p could target xCT. At the same time, it was also confirmed

that hsa_circ_0018189 could regulate xCT expression through miR-656-3p. Further studies confirmed that miR-656-3p inhibited tumorigenicity of cells by reducing the expression of xCT. Combining the research results, our study verified the targeting relationship between miR-656-3p, hsa_circ_0018189, and xCT in NSCLC for the first time. In conclusion, our study excavated a new regulatory pathway in the development of NSCLC by exploring the regulatory mechanism of new circRNA-miRNA-mRNA. Our study also provided new ideas for future drug development of NSCLC.

5 | CONCLUSION

In our study, hsa_circ_0018189 could regulate tumorigenicity of NSCLC through serving as a miR-656-3p sponge molecular and subsequently mediating xCT expression, which might be a potential target for the treatment of NSCLC.

ACKNOWLEDGEMENTS

None.

FUNDING INFORMATION

None.

CONFLICT OF INTEREST

The authors declare that they have no financial conflicts of interest.

DATA AVAILABILITY STATEMENT

Data sharing is not applicable to this article as no datasets were generated or analyzed during the current study.

ORCID

Yinghui Huang https://orcid.org/0000-0003-2574-1633

REFERENCES

1. Skřičková J, Kadlec B, Venclíček O, Merta Z. Lung cancer. *Cas Lek Cesk*. 2018;157(5):226-236.
2. McGuire A, Martin M, Lenz C, Sollano JA. Treatment cost of non-small cell lung cancer in three European countries: comparisons across France, Germany, and England using administrative databases. *J Med Econ*. 2015;18(7):525-532.
3. Kuhn E, Morbini P, Cancellieri A, Damiani S, Cavazza A, Comin CE. Adenocarcinoma classification: patterns and prognosis. *Pathologica*. 2018;110(1):5-11.
4. Santos ES, Hart L. Advanced squamous cell carcinoma of the lung: current treatment approaches and the role of Afatinib. *Onco Targets Ther*. 2020;13:9305-9321.
5. Osmani L, Askin F, Gabrielson E, Li QK. Current WHO guidelines and the critical role of immunohistochemical markers in the subclassification of non-small cell lung carcinoma (NSCLC): moving from targeted therapy to immunotherapy. *Semin Cancer Biol*. 2018;52(Pt 1):103-109.
6. Dubin S, Griffin D. Lung cancer in non-smokers. *Mo Med*. 2020;117(4):375-379.
7. Yu X, Li J, Zhong X, He J. Combination of Iodine-125 brachytherapy and chemotherapy for locally recurrent stage III non-small cell lung cancer after concurrent chemoradiotherapy. *BMC Cancer*. 2015;15(1):656.
8. Cheung CHY, Juan HF. Quantitative proteomics in lung cancer. *J Biomed Sci*. 2017;24(1):37.
9. Mumtaz P, Taban Q, Dar M, et al. Deep insights in circular RNAs: from biogenesis to therapeutics. *Biol Proced Online*. 2020;22:10.
10. Lu Y, Li Z, Lin C, Zhang J, Shen Z. Translation role of circRNAs in cancers. *J Clin Lab Anal*. 2021;35(7):e23866.
11. Zhao W, Zhang Y, Zhu Y. Circular RNA circβ-catenin aggravates the malignant phenotype of non-small-cell lung cancer via encoding a peptide. *J Clin Lab Anal*. 2021;35(9):e23900.
12. Chen X, Mao R, Su W, et al. Circular RNA circHIPK3 modulates autophagy via MIR124-3p-STAT3-PRKAA/AMPKα signaling in STK11 mutant lung cancer. *Autophagy*. 2020;16(4):659-671.
13. Yang B, Zhao F, Yao L, Zong Z, Xiao L. CircRNA circ_0006677 inhibits the progression and glycolysis in non–small-cell lung cancer by sponging miR-578 and regulating SOCS2 expression. *Front Pharmacol*. 2021;12(839):657053.
14. Wan J, Hao L, Zheng X, Li Z. Circular RNA circ_0020123 promotes non-small cell lung cancer progression by acting as a ceRNA for miR-488-3p to regulate ADAM9 expression. *Biochem Biophys Res Commun*. 2019;515(2):303-309.
15. Yao JT, Zhao SH, Liu QP, et al. Over-expression of CircRNA_100876 in non-small cell lung cancer and its prognostic value. *Pathol Res Pract*. 2017;213(5):453-456.
16. Martín J, Castellano JJ, Marrades RM, et al. Role of the epithelial-mesenchymal transition-related circular RNA, circ-10720, in non-small-cell lung cancer. *Transl Lung Cancer Res*. 2021;10(4):1804-1818.
17. Yang Z, Wang L. Regulation of microRNA expression and function by nuclear receptor signaling. *Cell Biosci*. 2011;1(1):31.
18. Liu H, Lei C, He Q, Pan Z, Xiao D, Tao Y. Nuclear functions of mammalian MicroRNAs in gene regulation, immunity and cancer. *Mol Cancer*. 2018;17(1):64.
19. Pauley KM, Cha S, Chan EK. MicroRNA in autoimmunity and autoimmune diseases. *J Autoimmun*. 2009;32(3–4):189-194.
20. Garzon R, Calin GA, Croce CM. MicroRNAs in cancer. *Annu Rev Med*. 2009;60:167-179.
21. Farazi TA, Spitzer JI, Morozov P, Tuschl T. miRNAs in human cancer. *J Pathol*. 2011;223(2):102-115.
22. Zhu X, Kudo M, Huang X, et al. Frontiers of MicroRNA signature in non-small cell lung cancer. *Front Cell Dev Biol*. 2021;9:643942.
23. Han Y, Li H. miRNAs as biomarkers and for the early detection of non-small cell lung cancer (NSCLC). *J Thorac Dis*. 2018;10(5):3119-3131.
24. Wang R, Wang ZX, Yang JS, Pan X, De W, Chen LB. MicroRNA-451 functions as a tumor suppressor in human non-small cell lung cancer by targeting ras-related protein 14 (RAB14). *Oncogene*. 2011;30(23):2644-2658.
25. Shih AY, Murphy TH. xCt cystine transporter expression in HEK293 cells: pharmacology and localization. *Biochem Biophys Res Commun*. 2001;282(5):1132-1137.
26. Ji X, Qian J, Rahman SMJ, et al. xCT (SLC7A11)-mediated metabolic reprogramming promotes non-small cell lung cancer progression. *Oncogene*. 2018;37(36):5007-5019.
27. Habib E, Linher-Melville K, Lin HX, Singh G. Expression of xCT and activity of system xc(−) are regulated by NRF2 in human breast cancer cells in response to oxidative stress. *Redox Biol*. 2015;5:33-42.
28. Livak KJ, Schmittgen TD. Analysis of relative gene expression data using real-time quantitative PCR and the 2(-Delta Delta C[T]) method. *Methods*. 2001;25(4):402-408.
29. Hori K, Shiota G, Kawasaki H. Expression of hepatocyte growth factor and c-met receptor in gastric mucosa during gastric ulcer healing. *Scand J Gastroenterol*. 2000;35(1):23-31.
30. Han Y, Xu GX, Lu H, et al. Dysregulation of miRNA-21 and their potential as biomarkers for the diagnosis of cervical cancer. *Int J Clin Exp Pathol*. 2015;8(6):7131-7139.
31. Rotow J, Bivona TG. Understanding and targeting resistance mechanisms in NSCLC. *Nat Rev Cancer*. 2017;17(11):637-658.

32. Mielgo-Rubio X, Uribelarrea EA, Cortés LQ, Moyano MS. Immunotherapy in non-small cell lung cancer: update and new insights. *J Clin Transl Res*. 2021;7(1):1-21.
33. Chen L, Shan G. CircRNA in cancer: fundamental mechanism and clinical potential. *Cancer Lett*. 2021;505:49-57.
34. Tang SJ, Yang JB. LncRNA SNHG14 aggravates invasion and migration as ceRNA via regulating miR-656-3p/SIRT5 pathway in hepatocellular carcinoma. *Mol Cell Biochem*. 2020;473(1–2):143-153.
35. Tian X, Liu Y, Wang Z, Wu S. lncRNA SNHG8 promotes aggressive behaviors of nasopharyngeal carcinoma via regulating miR-656-3p/SATB1 axis. *Biomed Pharmacother*. 2020;131:110564.
36. Zhang B, Gao S, Bao Z, Pan C, Tian Q, Tang Q. MicroRNA-656-3p inhibits colorectal cancer cell migration, invasion, and chemoresistance by targeting sphingosine-1-phosphate phosphatase 1. *Bioengineered*. 2022;13(2):3810-3826.
37. Chen T, Qin S, Gu Y, Pan H, Bian D. Long non-coding RNA NORAD promotes the occurrence and development of non-small cell lung cancer by adsorbing MiR-656-3p. *Mol Genet Genomic Med*. 2019;7(8):e757.
38. Hu K, Li K, Lv J, et al. Suppression of the SLC7A11/glutathione axis causes synthetic lethality in KRAS-mutant lung adenocarcinoma. *J Clin Invest*. 2020;130(4):1752-1766.

SUPPORTING INFORMATION

Additional supporting information can be found online in the Supporting Information section at the end of this article.

How to cite this article: Cai J, Zheng Y, Dong L, Zhang X, Huang Y. Circular RNA hsa_circ_0018189 drives non-small cell lung cancer growth by sequestering miR-656-3p and enhancing xCT expression. *J Clin Lab Anal*. 2022;36:e24714. doi: 10.1002/jcla.24714